Experimental Study on Tensile Behavior of Wet Joints in a Prefabricated Composite Deck System Composed of Orthotropic Steel Deck and Ultrathin Reactive-Powder Concrete Layer

Wen-Hao Pan[1]; Jian-Sheng Fan[2]; Jian-Guo Nie[3]; Jian-Hua Hu[4]; and Jian-Feng Cui[5]

Abstract: The widely used orthotropic steel deck system is subject to several durability problems: fatigue cracking of the steel, wearing of the surfacing, and corrosion. Thus, the composite deck system composed of an orthotropic steel deck and an ultrathin reactive-powder concrete (RPC) layer was proposed. In a prefabricated composite deck system, joints formed between the prefabricated RPC layer and the cast-in-situ RPC layer are defined as wet joints. The experimental study was conducted on the tensile behavior of RPC wet joints to ensure the integrity of the prefabricated deck system and the serviceability and durability of the RPC layer. Two series of tests were conducted, including seven tensile tests on panels and four negative bending tests on beams. In these tests, five types of new wet joint details were designed in addition to the integral casting detail and the conventional wet joint with a vertical, plane interface. To study the mechanical properties and crack resistance performance of different wet joint details, the load-deformation curves and the nominal RPC tensile stress–maximum crack width curves of the models in each test series were compared. Comparisons showed that the mechanical properties of different wet joint details were close to one another. However, their crack resistance performance differed considerably. The sawtooth wet joint, rectangular wet joint, and steel plate–enhanced wet joint had substantially better crack resistance performance than the conventional wet joint. In contrast, the inclined wet joint and the reinforcement-enhanced wet joint had poor crack resistance performance because of their plane interfaces. Additionally, test results suggested that the postcracking behavior of the RPC layer was improved by the steel fibers. Therefore, for more economical bridge designs, the durability-based allowable RPC tensile stress was recommended instead of the initial cracking stress. **DOI: 10.1061/(ASCE)BE.1943-5592.0000935.**

Author keywords: Prefabricated composite deck system; Orthotropic steel deck system; Reactive-powder concrete (RPC); Wet joint; Tensile behavior; Crack width.

Introduction

The two essential conditions for economic steel bridge designs are an efficient load transfer mechanism and a considerably reduced dead weight (Wolchuk 1963). These conditions result in the design of the conventional orthotropic steel deck system [Fig. 1(a)], which is widely used in long-span bridges, especially suspension bridges and cable-stayed bridges (AASHTO 2012; Connor et al. 2012; Wolchuk 1963). However, this steel deck system is subject to several durability problems: fatigue cracking of the steel (de Jong 2004; Walter et al. 2007; Wolchuk 1999), wearing of the surfacing (Wolchuk 1999, 2002), and corrosion (Buitelaar et al. 2004; Hulsey et al. 1999; Rafiee 2012). The main reasons for fatigue cracking of the steel are (1) large local deformations and stresses caused by the wheel loads resulting from insufficient stiffness of the steel deck plate, and (2) excessive stress concentration resulting from inappropriate details, especially in close-rib decks (Wolchuk 1999). The main reasons for wearing of the surfacing are (1) incompatibility of the surfacing with the local deformations of the steel deck plate, and (2) insufficient bond strength between the surfacing and the steel deck plate. The main reason for corrosion is the poor corrosion resistance of steel.

A composite deck system [Fig. 1(b)] composed of an orthotropic steel deck and an ultrathin reactive-powder concrete (RPC) layer was proposed by Shao et al. (2013) to solve the two durability problems in the conventional orthotropic steel deck system. RPC is a high-performance fiber-reinforced concrete with high compressive and flexure strength and good ductility (Richard and Cheyrezy 1995). As shown in Fig. 1, the thick conventional asphalt surfacing was changed into the RPC layer and an ultrathin high-performance asphalt surfacing in the composite deck system. The composite action between steel and RPC was realized with shear connectors. Thus, the stiffness of the steel deck plate was largely improved in the new deck system, and the low self-weight of the structure was

[1]Ph.D. Candidate, Beijing Engineering Research Center of Steel and Concrete Composite Structures, Dept. of Civil Engineering, Tsinghua Univ., Beijing100084, China. E-mail: panwenhao13@tsinghua.org.cn

[2]Professor, Beijing Engineering Research Center of Steel and Concrete Composite Structures, Dept. of Civil Engineering, Tsinghua Univ., Beijing100084, China (corresponding author). E-mail: fanjsh@tsinghua.edu.cn

[3]Professor, Key Laboratory of Civil Engineering Safety and Durability of China Education Ministry, Dept. of Civil Engineering, Tsinghua Univ., Beijing 100084, China. E-mail: niejg@mail.tsinghua.edu.cn

[4]Professor, Hunan Provincial Communications Planning, Survey and Design Institute, College of Civil Engineering, Hunan Univ., Hunan 410082, China. E-mail: hujianhua2009@163.com

[5]Ph.D. Candidate, College of Civil Engineering, Hunan Univ., Hunan 410082, China. E-mail: 274834365@qq.com

Note. This manuscript was submitted on October 15, 2015; approved on March 15, 2016; published online on April 15, 2016. Discussion period open until September 15, 2016; separate discussions must be submitted for individual papers. This paper is part of the ***Journal of Bridge Engineering***, © ASCE, ISSN 1084-0702.

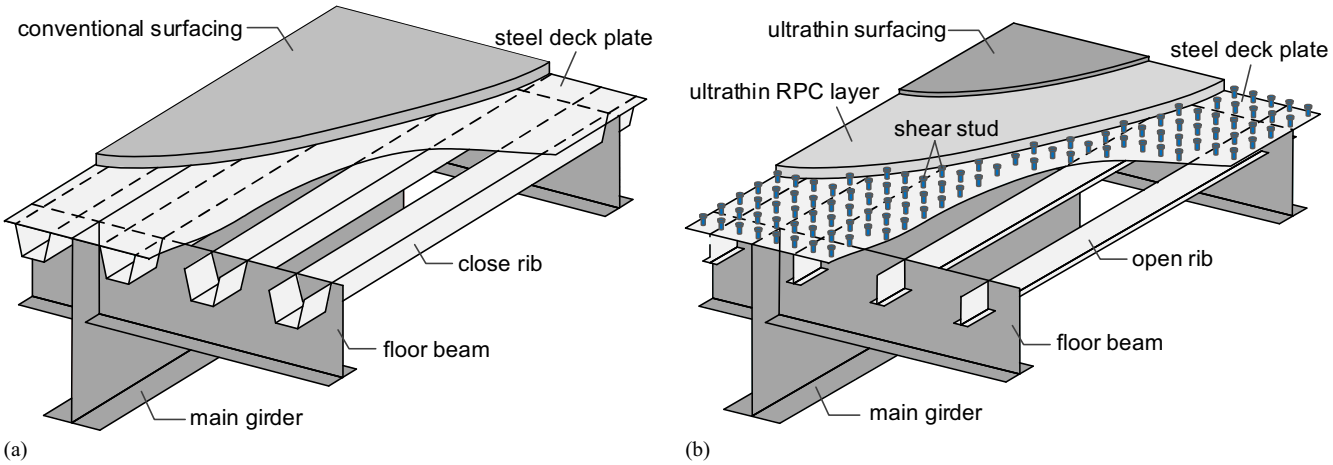

Fig. 1. (a) Conventional orthotropic steel deck system; (b) composite deck system

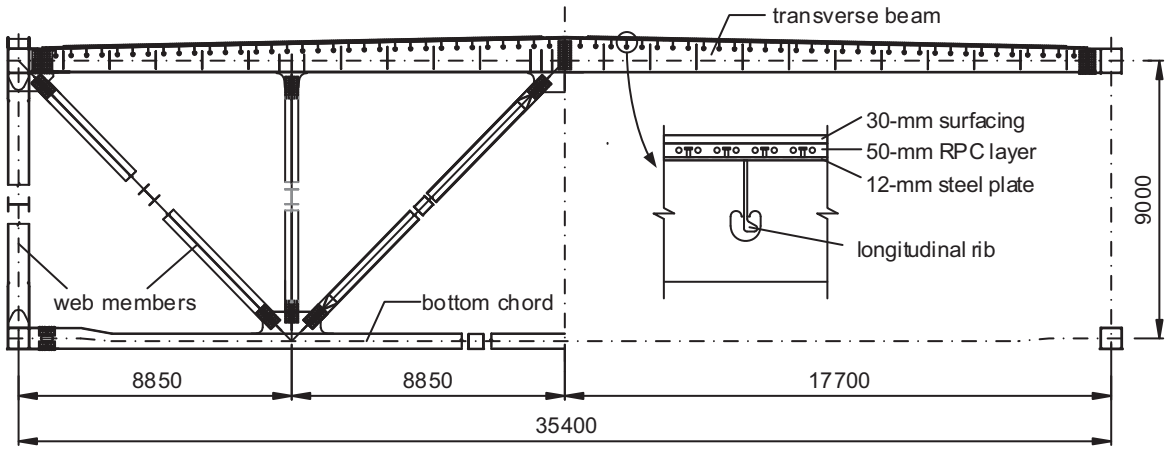

Fig. 2. Typical girder cross section of Dongting Lake Second Bridge (Note: All dimensions are in millimeters)

maintained. Because the RPC layer was sufficient to distribute loads in the transverse direction, the open longitudinal ribs were applied to reduce the excessive stress concentration in close-rib decks. Therefore, by increasing the stiffness of the steel deck plate, by reducing the excessive stress concentration in close-rib deck details, and by providing sufficient bond strength between the surfacing and the RPC layer, the composite deck system can solve the problems of fatigue cracking of the steel and wearing of the surfacing. Additionally, because of the good corrosion resistance of RPC (Buitelaar et al. 2004; Rafiee 2012), the corrosion resistance of the bridge system can be improved.

A 1,480-m-span cable-stayed bridge called the Dongting Lake Second Bridge is being built in the Hunan Province of China. The bridge uses the composite deck system, and a typical girder cross-section of the bridge is shown in Fig. 2. To ensure construction quality in a short time period, the bridge girder segments, including the RPC layers, are prefabricated. During construction, the steel members in two adjacent prefabricated girder segments are bolted together, and the RPC layers are connected by a cast-in-situ RPC layer. Thus, joints are formed between the prefabricated RPC layer and the cast-in-situ RPC layer and are defined as wet joints. Because few steel fibers lie in the interfaces between the prefabricated and the cast-in-situ RPC layer, crack development in the conventional RPC wet joint with a vertical, plane interface may not be controlled well. Therefore, for the integrity of the bridge and the serviceability and durability of the RPC layer, wet joint details with better mechanical properties and crack resistance performance need to be developed.

In this study, six different RPC wet joint details and the integral casting details were compared through two series of tests: a tensile test series on panels and a negative bending test series on beams. During the tests, the maximum crack width in the RPC surface was measured. Then, the load-deformation curves were compared to study the mechanical properties of different wet joints, and the nominal RPC tensile stress-maximum crack width curves were compared to study the crack resistance performance. Finally, durability-based allowable RPC tensile stresses were calculated and recommended for more economical bridge designs.

Experimental Program

Details of Test Models

Based on the Dongting Lake Second Bridge, two series of test models were designed, including seven panels and four beams.

Details of the panels are shown in Fig. 3. The panels were $1{,}200 \times 450 \times 62$ mm in size. Each panel consisted of a 12-mm thick steel plate and a 50-mm-thick ultrathin RPC layer. The test

setup included end plates on two ends of the panels. The steel plate and the reinforcements in the RPC layer were all welded to the end plates. As shown in Fig. 3(a), three types of longitudinal reinforcements were placed in the RPC layer: full-length reinforcements, central reinforcements, and end reinforcements. The central reinforcements placed in the central wet joint region were designed to improve the tensile behavior of wet joints, and the end reinforcements were designed to transfer loads from the end plates to the RPC layer.

Details of the beams are shown in Fig. 4. The beams were steel-RPC composite beams with an overall depth of 400 mm. The steel tensile flange and the RPC layer were consistent with the panels. Also, the full-length reinforcements and the central reinforcements were placed in the RPC layer as shown in Fig. 4(a).

In all test models, a type of short shear stud, as shown in Fig. 5, was used at a spacing of 125×120 mm to ensure the composite action between steel and RPC. The diameter and height of the shear stud were 13 and 35 mm, respectively.

Details of Wet Joints

Fig. 6 shows different RPC wet joint details in the test models; additional details are shown in Table 1. As shown in Fig. 6, the test models with wet joints were casted in two steps, representing the prefabricated and the cast-in-situ RPC layers in the original bridge. Before casting the second half of the RPC layer, the prefabricated half was surface roughened after demolding (Fig. 7) to expose some steel

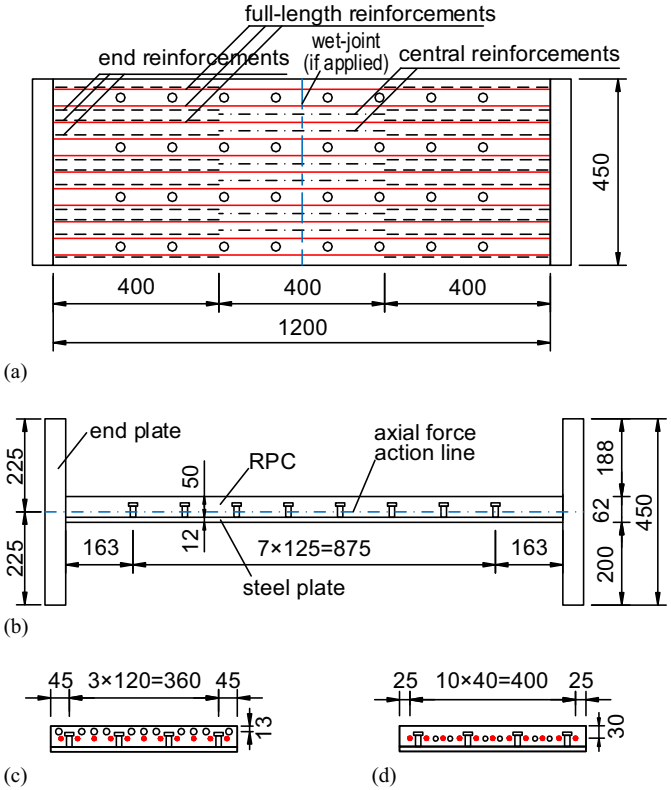

Fig. 3. Details of panels: (a) plan view; (b) elevation (Note: All dimensions are in millimeters)

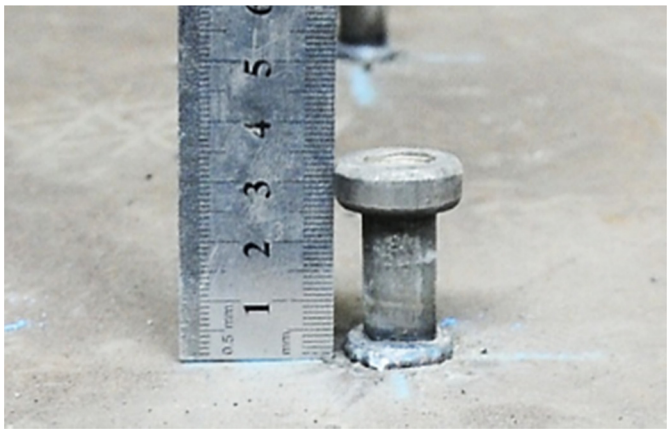

Fig. 5. Short shear stud

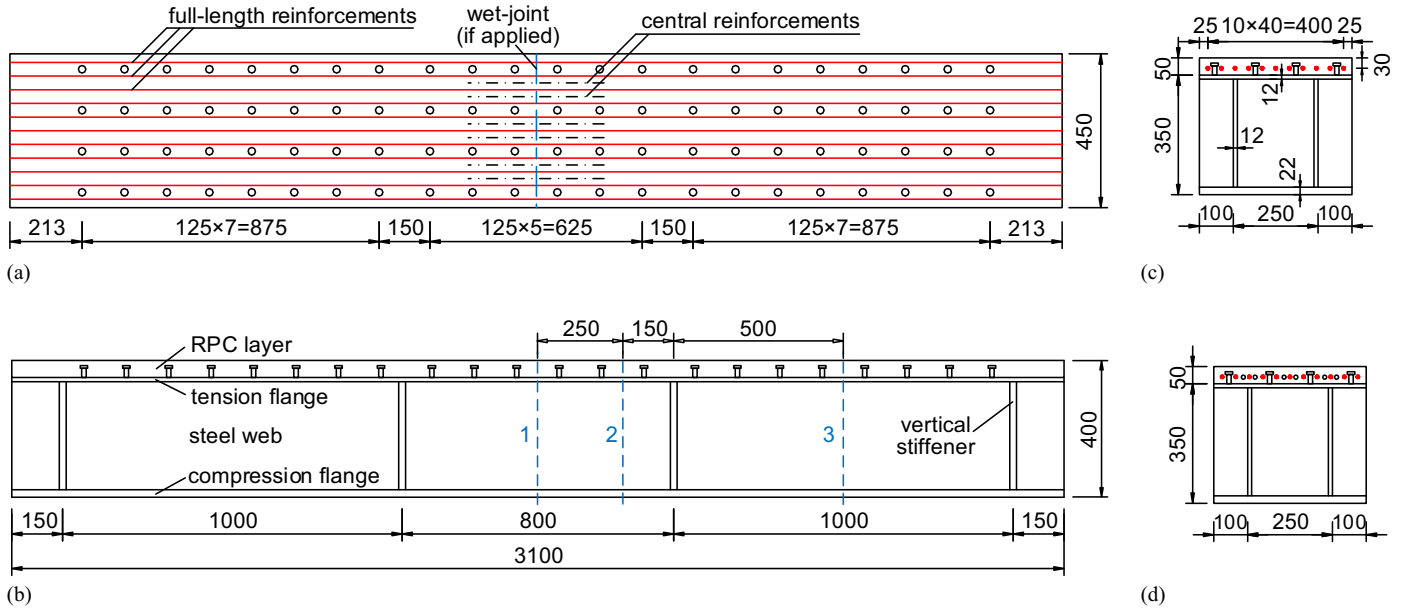

Fig. 4. Details of beams: (a) plan view; (b) elevation (Note: All dimensions are in millimeters)

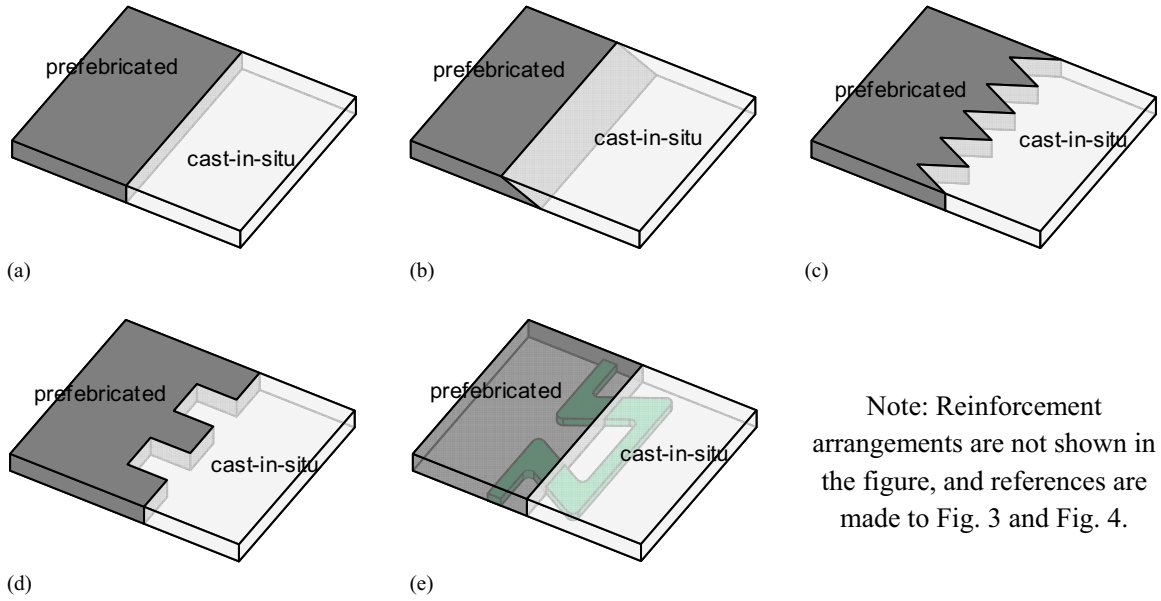

Fig. 6. Different wet joint details: (a) conventional wet joint; (b) inclined wet joint; (c) sawtooth wet joint; (d) rectangular wet joint; (e) steel plate–enhanced wet joint

Table 1. Wet Joint Details in Test Models

Wet joint	Details	Reinforcing rebar ratio in wet joint (%)	Reinforcing steel plate ratio in wet joint (%)	Panel	Beam
Integral casting detail	Integral casting	3.84	0	RPC-T-1	RPC-B-1
Conventional wet joint	Vertical, plane interface	6.86	0	RPC-T-2	RPC-B-2
Reinforcement-enhanced wet joint	Conventional wet joint enhanced by larger full-length reinforcements	10.54	0	RPC-T-3	—
Inclined wet joint	Inclined interface	6.86	0	RPC-T-4	—
Sawtooth wet joint	Sawtooth interface	6.86	0	RPC-T-5	RPC-B-3
Rectangular wet joint	Rectangular interface	6.86	0	RPC-T-6	RPC-B-4
Steel plate-enhanced wet joint	Conventional wet joint enhanced by a 14-mm-thick specially shaped steel plate	3.84	8.96	RPC-T-7	—

Fig. 7. Surface roughening after demolding

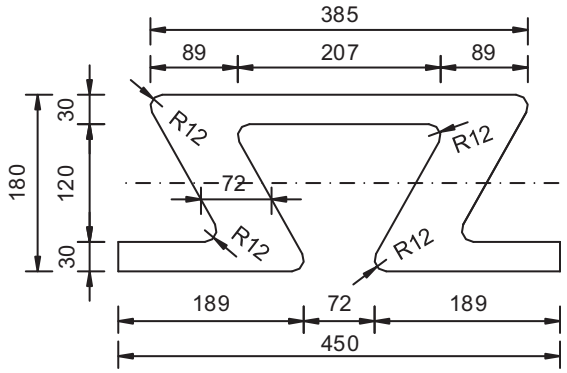

Fig. 8. Specially shaped steel plate (Note: All dimensions are in millimeters)

fibers. In addition to the integral casting detail and the conventional wet joint used as reference tests, five types of new wet joint details were designed. Three wet joints changed the shape of the wet joint interfaces into inclined shape, sawtooth shape, and rectangular shape, respectively, whereas the other two wet joints enhanced their plane interfaces by using larger full-length reinforcements and specially shaped steel plates (Fig. 8). Additionally, it should be noted that the central reinforcements for wet joints were canceled in the integral casting detail and the steel plate–enhanced wet joint.

Except for wet joint details, the models in each test series were identical. In the tensile test series on panels, panels with all five new

wet joint details were designed. In the bending test series on beams, only the sawtooth wet joint and the rectangular wet joint were studied in addition to the integral casting detail and the conventional wetjoint.

Loading Method and Instrumentation

All panels were tested using a 10,000-kN tensile tester, as shown in Fig. 9. The tensile load was transferred to the test panel through two articulated joints, so that no additional bending moment was applied to the panel cross section in the axial force action line [Fig. 3(b)]. It should be noted that the axial force action line was designed to be closer to the RPC surface than the centroid of the panel cross section. Thus, initial cracks would first appear in the RPC surface, so that crack observations were facilitated. During the tensile tests on panels, an unloading and reloading cycle was designed. The panels were first loaded to 750 kN when the nominal RPC tensile stress (see the later section on nominal RPC tensile stress) was approximately 20 MPa, and were then unloaded to 0 kN before being reloaded to failure. The load was increased at an increment of 50 kN and was kept constant at each step to measure the crack width in the RPC surface.

The test setup used to perform the bending tests on beams is shown in Fig. 10. The beams were tested to failure using two symmetric point loads that produce a constant negative moment region. The length of the constant moment region was 800 mm. Vertical stiffeners were designed at the supports and the loading points to prevent local buckling of the steel web before flexural failure. Also, the crack width was measured at every load increment of 50 kN.

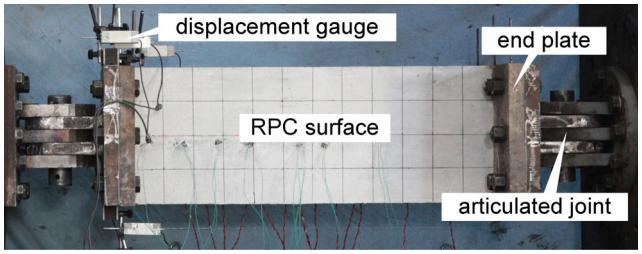

Fig. 9. Test setup for panels

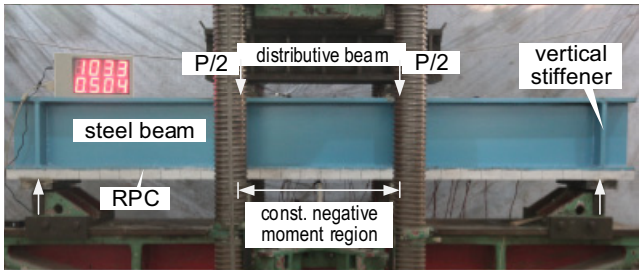

Fig. 10. Test setup for beams

Material Properties

Material properties with respect to steel, rebar, and RPC are summarized in Tables 2 and 3. The mix proportion of the RPC material is shown in Table 4. A mixture of two types of steel fibers was applied in the RPC material. One type had a diameter of 0.12 mm and a length of 8 mm, and the other type had a diameter of 0.2 mm and a length of 13 mm. Their volume ratios were 1.5% and 2%, respectively. The tensile strength of both types of steel fibers was 2,700 MPa. Additionally, a 90°C hot-steam curing was performed for 48 h after the initial setting of the RPC. The elastic modulus of the RPC material was 42,600 MPa (Shao et al. 2013).

Tensile Tests on Panels

Test Observations

Test observations of the panels are as follows. As the load increased gradually, initial tensile cracks formed in the transverse direction of the RPC surface. The cracking loads, cracking stresses, and cracking strains of these panels are shown in Table 5. After initial cracking, new cracks started to appear and developed continuously. The crack

Table 3. Material Properties of RPC

Application	f_{cu} (MPa)	f_r (MPa)	f_{cr} (MPa)
Prefabricated half	155.2	29.5	13.6
Cast-in-situ half	155.7	28.6	12.9

Note: f_{cu} = cubic compressive strength determined by 100 × 100 × 100 mm specimens; f_r and f_{cr} = flexural strength and cracking stress determined by four-point bending test of 100 × 100 × 400 mm specimens, respectively.

Table 4. Mix Proportion of RPC for Test Models

Material	Mass ratio
Cement	1
Quartz sand	1.1
Silica fume	0.2
Fly ash	0.1
Quartz powder	0.2
Water	0.19
Water reducer	1.5%
Steel fiber volume ratio (L = 8 mm)	1.5%
Steel fiber volume ratio (L = 13 mm)	2%

Table 2. Material Properties of Steel and Rebar

Material	Applications	Thickness/diameter (mm)	f_y (MPa)	f_u (MPa)
Q345 steel	Steel plate and steel beam	12	392.2	552.0
		22	346.4	551.3
HRB400 rebar	Full-length reinforcements	Φ10	509.3	611.2
	Central reinforcements	Φ12	530.5	654.3
	Full-length reinforcements in RPC-T-3	Φ14	441.7	597.6
	End reinforcements in panels	Φ16	467.5	581.9

Note: f_y = yield stress; f_u = ultimate stress.

Table 5. Test Results of Panels

Panel	P_{cr} (kN)	σ_{cr} (MPa)	ε_{cr} ($\mu\varepsilon$)	P_{failure} (kN)
RPC-T-1	450	11.8	370	1,109
RPC-T-2	100	2.6	94	1,714
RPC-T-3	300	7.9	272	1,446
RPC-T-4	250	6.6	223	1,804
RPC-T-5	375	9.8	306	1,849
RPC-T-6	400	10.5	315	2,262
RPC-T-7	400	10.5	310	2,405

Note: P_{cr} = cracking load; σ_{cr} = cracking stress (i.e., the nominal RPC tensile stress at cracking load); ε_{cr} = cracking strain measured by a strain gauge; P_{failure} = failure load.

development was accompanied by a small sound, which was probably caused by the microcracking of the RPC matrix and the debonding between steel fibers and RPC at local regions (Li et al. 1993). In all test panels, failure occurred shortly after the sudden rupture of the reinforcement–end plate welding (Fig. 11). As a result of the discreteness of the welding process, the failure loads ranged from 1,109 to 2,405 kN (Table 5).

The crack distributions of the panels after testing are shown in Fig. 12. Because of the weak adhesion between RPC and the end plate, the RPC layer in the end region did not fully participate in bearing the tensile load. Therefore, the cracks were mainly distributed in the 400-mm-long central wet joint region. Additionally, because the cracks were well developed, the test results in the test series were sufficient for this study, although all the test panels failed as a result of the failure of the test setup.

Test Results

The load-axial deformation curves of the panels are shown in Fig. 13. The initial stiffnesses of the panels were close to one another because they were identical except for the wet joint details. As the load increased gradually, the stiffness of these panels started to decrease as a result of crack development. However, no significant stiffness degradation was discovered because the RPC layer could still bear the tensile load with the steel fibers. After the unloading and reloading cycle, the deformations were nearly the same as before unloading, which suggested that the cracks had nearly no propagation during the load cycle. Because of the rupture of the reinforcement–end plate welding, sudden increases in axial deformations were observed at the failure loads.

The variations of longitudinal strains in RPC and steel along the panels are shown in Fig. 14 and Fig. 15, respectively. As a result of measurement system malfunction, the strain data of Panel RPC-T-4 was not collected. As shown in Fig. 14, the RPC strains in the central region (400–800 mm distance to end plate) were considerably larger than that in the end region because of cracking. In the end region, however, because the RPC layer did not fully participate in bearing the tensile load, the steel plate carried more loads. Therefore, the steel strains in the end region were larger than those in the central region, as shown in Fig. 15.

Bending Tests on Beams

Test Observations

Test observations of the beams are as follows. As the load increased gradually, initial tensile cracks started to appear. The cracking loads, cracking stresses, and cracking strains of these beams are shown in Table 6. Similar to the tensile tests on panels, further crack development was accompanied by a small sound that was probably caused by the microcracking of the RPC matrix and the debonding between steel fibers and RPC at local regions. The crack development can be divided into two stages: the average cracking stage before yielding of the steel beam and the concentrating cracking stage afterward. The average cracking stage was characterized by the gradual appearance of uniformly distributed hairline cracks in the RPC material, whereas the concentrating cracking stage was characterized by the formation of several concentrated cracks. After yielding of the steel beam, the midspan deflections of the beams increased rapidly, whereas nearly no strength degradation occurred. In all test beams, ductile, tension-controlled failures were observed.

Fig. 11. Rupture of reinforcement–end plate welding

The crack distributions of the beams after testing are shown in Fig. 16. In all test beams, the cracks were mainly distributed in the constant moment region because of a relatively high bending moment. The cracks can be classified into two categories: the main cracks and the secondary cracks. The main cracks were the concentrated cracks formed after yielding of the steel beam, and the secondary cracks were hairline cracks in the RPC material that appeared in the average cracking stage. Additionally, as shown in Fig. 16, no concentrated crack formed in the 400-mm-long central wet joint regions of Beams RPC-B-2–RPC-B-4 because of the higher longitudinal reinforcement ratio.

Test Results

The load-deflection curves of the beams at midspan are shown in Fig. 17. At the initial stage of loading (i.e., within 80% of P_u), the responses were linear and the stiffness of the beams did not decrease notably despite the crack development. The load-deflection curves were identical for different wet joint details before yielding of the steel beams. After yielding, significant stiffness degradations occurred. Then, the beams reached their ultimate loads at large midspan deflections (approximately 3–4 times the yielding deflections). The ultimate load of Beam RPC-B-2 with the conventional wet joint was 2,584 kN, which was only a 10.5% reduction of that for the integral casting Beam RPC-B-1. The ultimate loads of Beams RPC-B-3–RPC-B-4, which had better wet joint details, fell between those of RPC-B-1 and RPC-B-2. This suggests that the mechanical properties of different wet joint details were not significantly different because the wet joints were enhanced by the central reinforcements placed in the central wet joint region.

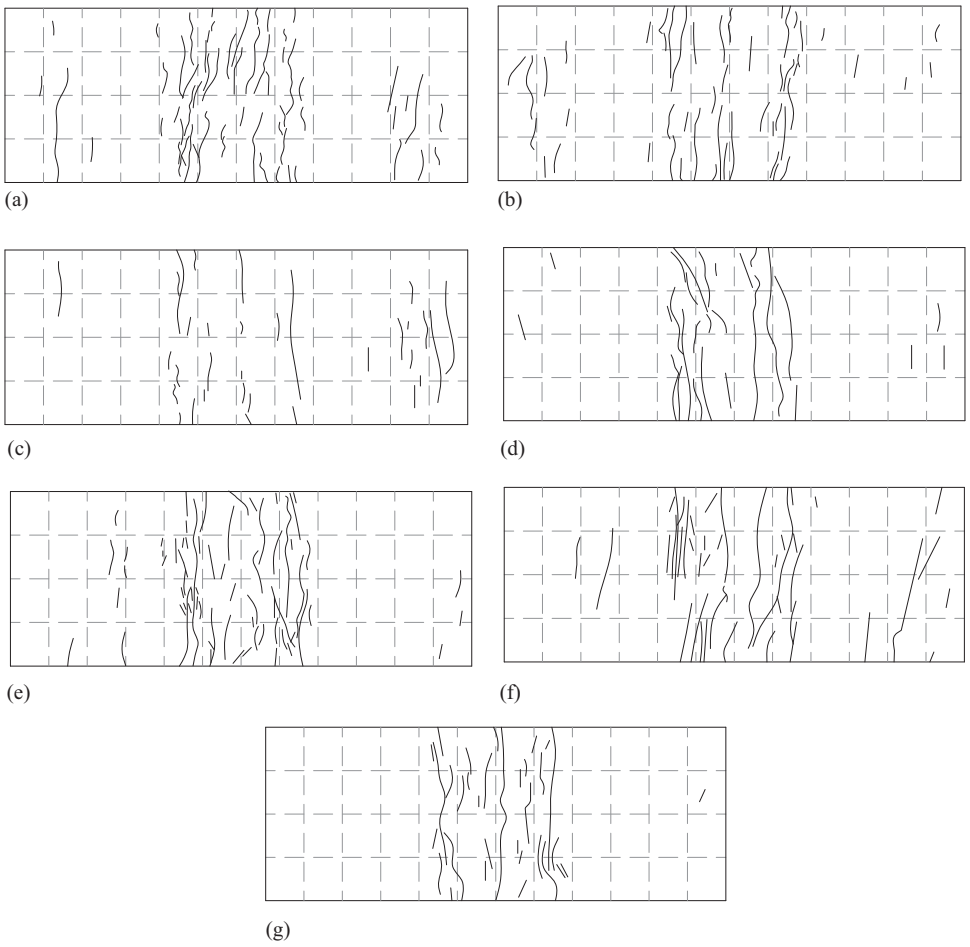

Fig. 12. Crack distributions of panels: (a) RPC-T-1; (b) RPC-T-2; (c) RPC-T-3; (d) RPC-T-4; (e) RPC-T-5; (f) RPC-T-6; (g) RPC-T-7

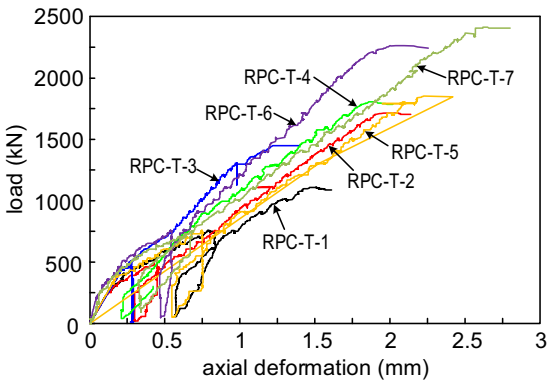

Fig. 13. Load-axial deformation curves of panels: (a) RPC-T-1; (b) RPC-T-2; (c) RPC-T-3; (d) RPC-T-5; (e) RPC-T-6; (f) RPC-T-7

The variations of longitudinal strains along the beam height in three typical cross sections [Fig. 4(b)] are shown in Fig. 18. Note that although initial RPC tensile cracks had already appeared when load = 1,000 kN, the measurements were still in good agreement with the elastic theory value based on the partial-interaction theory (see the later section on nominal RPC tensile stress). This result was consistent with the load-deflection responses that were linear within 80% of P_u despite the RPC cracking.

Discussion

Nominal RPC Tensile Stress

To study the crack resistance performance of different RPC wet joints, the nominal RPC tensile stress in the RPC surface was calculated for the two series of tests. In the stress calculation process, the test specimens were modeled elastically because the steel and rebar were in the elastic range and the RPC was either uncracked or in the microcracking stage (Bărbos and Păstrav 2014). Additionally, the rebar in the RPC layer should be considered in cross-section analyses. The elastic moduli of steel, rebar, and RPC are 210,000, 210,000, and 42,600 MPa, respectively. Note that test specimens in the RPC macrocracking stage are not included in this discussion because the RPC tangent modulus had decreased significantly.

For the panels, the plane section assumption was applied in the central wet joint region. Then, considering the elastic modulus ratio $n = E_s/E_c$ between steel and RPC, the nominal RPC tensile stress in the RPC surface can be formulated by the method of transformed sections (Johnson 2004).

$$\sigma_n = \frac{P}{nA_{0t}} + \frac{My_{ct}}{nI_{0t}} = \frac{P}{n}\left(\frac{1}{A_{0t}} + \frac{ey_{ct}}{I_{0t}}\right) \tag{1}$$

where P is the applied tensile load; $n = E_s/E_c$ is the elastic modulus ratio between steel and RPC; e is the distance between the tensile load action line and the centroid of the transformed panel cross

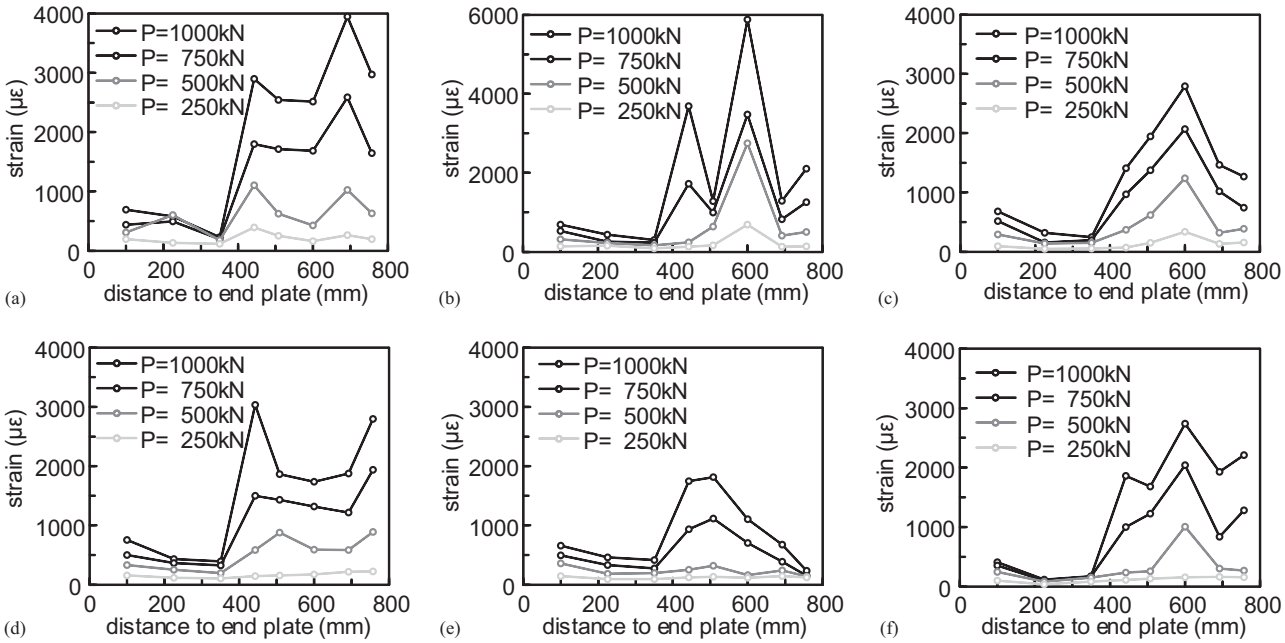

Fig. 14. Variation of RPC strains along panels

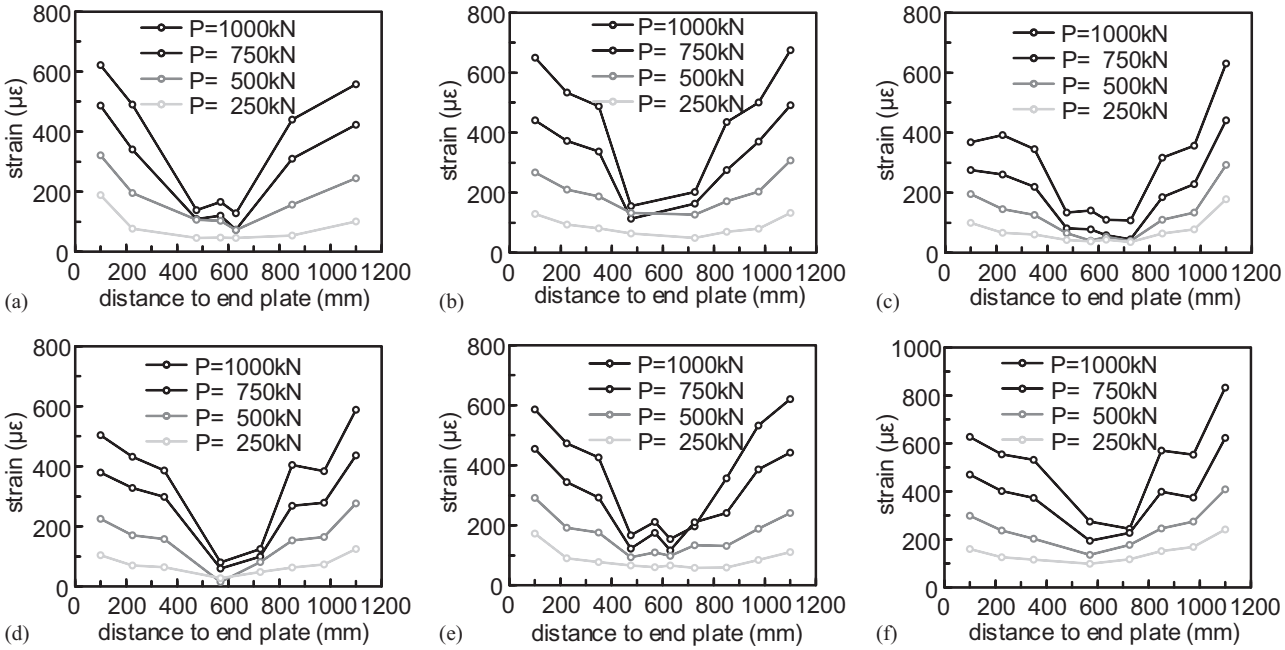

Fig. 15. Variation of steel strains along panels: (a) RPC-T-1; (b) RPC-T-2; (c) RPC-T-3; (d) RPC-T-5; (e) RPC-T-6; (f) RPC-T-7

section; y_{ct} is the distance between the RPC surface and the centroid of the transformed panel cross section; and A_{0t} and I_{0t} are the area and moment of inertia, respectively, of the transformed panel cross-section.

For the beams, however, the plane section assumption cannot be directly applied because the behavior of a composite beam may be modified by the presence of shear slip effect of the shear connectors (Johnson 2004; Nie et al. 2004). In this case, the partial-interaction theory (Johnson 2004; Wang 1998) is more suitable to correctly calculate the nominal RPC tensile stress, and the following assumptions were made: (1) the shear stress at the interface was proportional to the slip, and the shear connection (interface) stiffness was uniform and continuous along the length of the beams; (2) plane sections were assumed for the steel and RPC cross sections separately; and (3) the steel beam and RPC layer at the same section had the same curvature and rotation.

The first assumption gives the following slip equation:

$$v_L = \frac{Nk}{L}s \tag{2}$$

where s is the relative slip between steel and RPC; N is the number of rows of the shear stud; L is the longitudinal spacing of the shear stud; and k is the shear stiffness of shear stud, according to Wang (1998) and An and Cederwall (1996).

Fig. 19 shows in elevation a short beam element of length dx in the shear span. According to Assumptions (2) and (3), other equations regarding Fig. 19 can be deduced from equilibrium, elasticity, and compatibility. After solving these equations and inserting the boundary conditions for the shear span of the beam, the nominal RPC tensile stress in the RPC surface can be derived.

Comparisons of the strain test and theory results in the two test series are shown in Figs. 18 and 20. As shown in the two figures, the theory results are in good agreement with the test results. This indicates the good reliability and applicability of the nominal RPC tensile stress approach based on the plane section assumption and the partial-interaction theory.

Comparisons of Crack Resistance Performance

As noted in the discussion of test results, comparisons of the load-deformation curves of the models in each test series (Figs. 13 and 17) suggest that the mechanical properties of different wet joint details were not significantly different. This is the result of the enhancement of the wet joints by the central reinforcements placed in the central wet joint region. However, on a microlevel, the crack resistance performance of different wet joints may differ considerably. Therefore, the development of the maximum crack width relative to the nominal RPC tensile stress in the two test series was compared.

Table 6. Test Results of Beams

Panel	P_{cr} (kN)	σ_{cr} (MPa)	ε_{cr} ($\mu\varepsilon$)	P_u (kN)
RPC-B-1	900	16.0	986	2887
RPC-B-2	300	5.3	295	2584
RPC-B-3	600	10.7	596	2659
RPC-B-4	650	11.6	684	2744

Note: P_u = ultimate load.

The nominal RPC tensile stress–maximum crack width curves of the panels are shown in Fig. 21. The curves in the unloading and reloading cycle are not shown in the figure because nearly no crack propagation was observed during that cycle. As shown in Fig. 21, the maximum crack widths increased gradually with the increase in the nominal RPC tensile stresses. Comparisons of the seven curves indicated that the crack resistance performance of different wet joint details differed considerably. All of the other panels had better crack resistance performance than the reference panel, Panel RPC-T-2, with the conventional wet joint. Panels RPC-T-5–RPC-T-7 had crack resistance performance as good as that of the integral casting panel, Panel RPC-T-1, because of their good wet joint details; the crack propagations of panels RPC-T-5–RPC-T-7 were restricted well, although their nominal RPC cracking stresses were slightly smaller than that of panel RPC-T-1. In contrast, the crack resistance performance of Panel RPC-T-4 was poor as a result of the plane interface of the inclined wet joint, and its maximum crack width was considerably larger than that of the other panels, except Panel RPC-T-2. Compared with Panel RPC-T-4, the cracking stress of Panel RPC-T-3 was just as large, but its crack development was limited because of the enlarged full-length reinforcements.

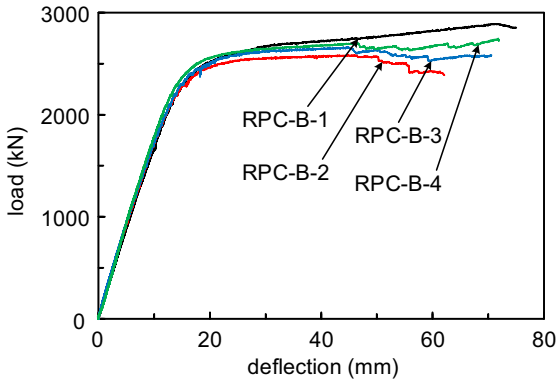

Fig. 17. Load-deflection curves of beams at midspan

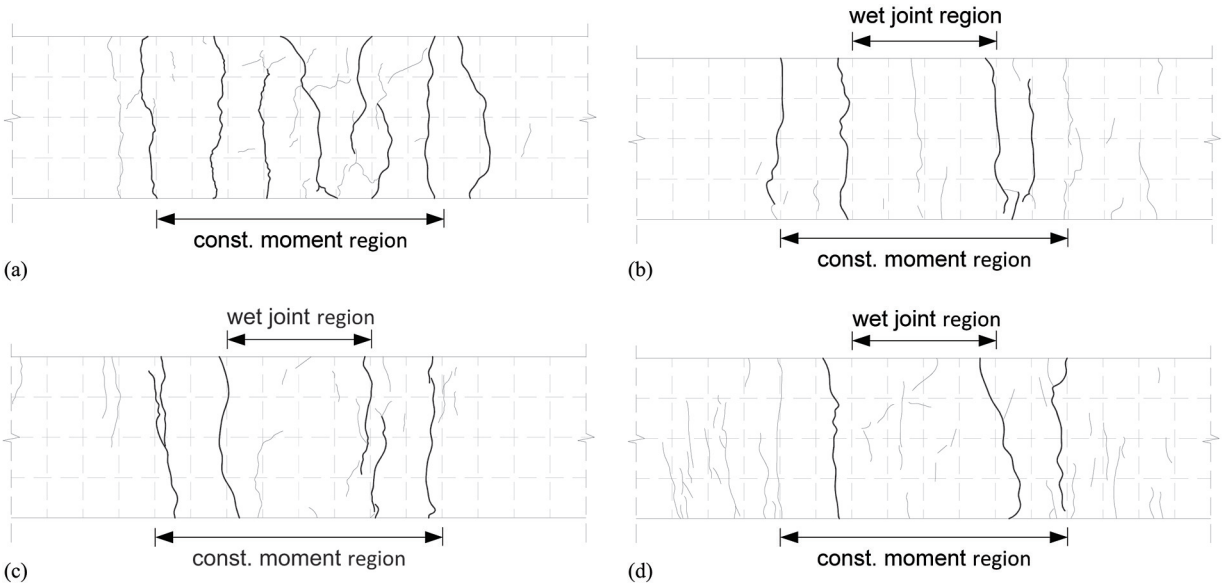

Fig. 16. Crack distributions of beams: (a) RPC-B-1; (b) RPC-B-2; (c) RPC-B-3; (d) RPC-B-4

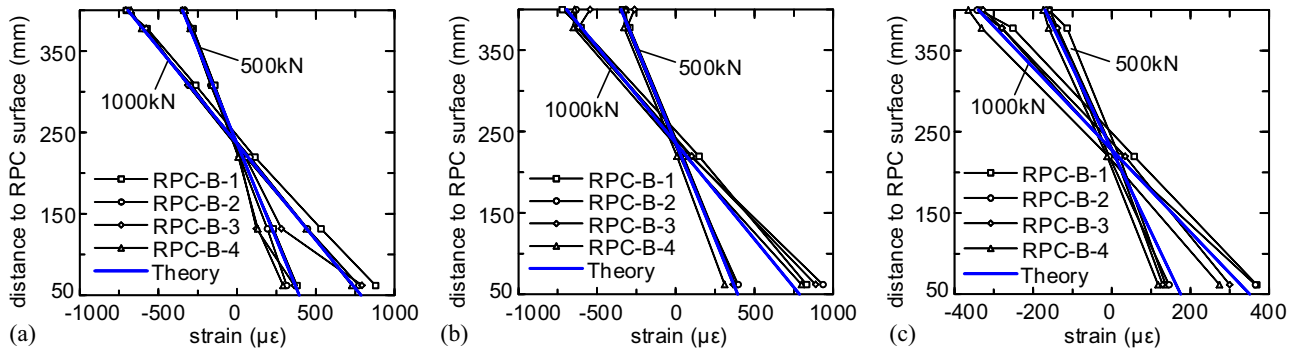

Fig. 18. Variation of strains along beam height: (a) Cross Section 1; (b) Cross Section 2; (c) Cross Section 3

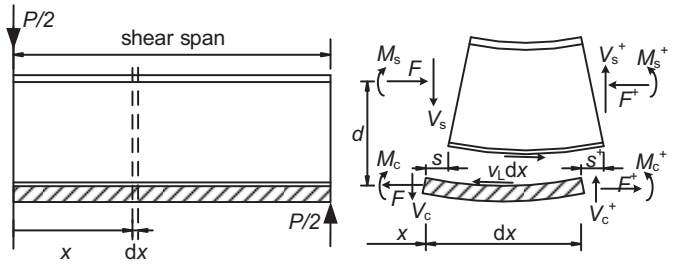

Fig. 19. Partial-interaction analysis of beams

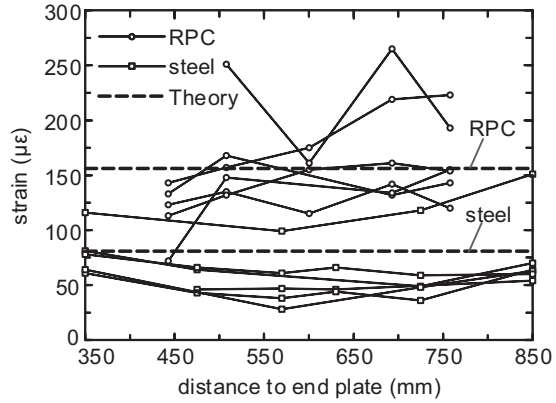

Fig. 20. Comparisons of strain test and theory results in panels (load = 250 kN)

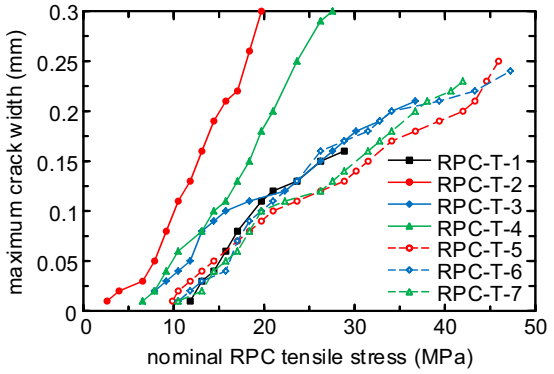

Fig. 21. Nominal RPC tensile stress–maximum crack width curves of panels

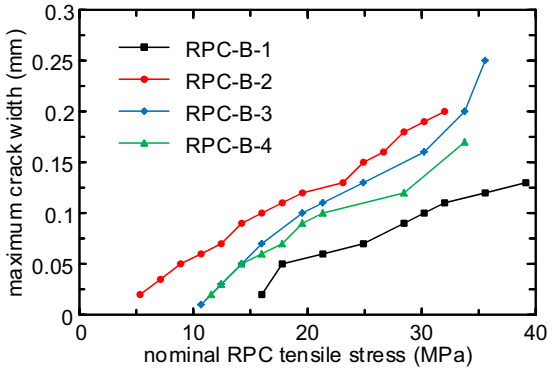

Fig. 22. Nominal RPC tensile stress–maximum crack width curves of beams

The nominal RPC tensile stress–maximum crack width curves of the beams are shown in Fig. 22. Initially, the maximum crack widths increased linearly with the increase of the nominal RPC tensile stresses. After yielding of the steel beam, concentration of cracking resulted in rapid increases in the maximum crack widths. Comparisons of the four curves indicated that Beam RPC-B-2 with the conventional wet joint had the worst crack resistance performance, whereas the integral casting beam, Beam RPC-B-1, had the best performance. Because of better wet joint details, the nominal RPC tensile stress–maximum crack width responses of beams RPC-B-3–RPC-B-4 were between those of RPC-B-1 and RPC-B-2.

Comparisons of initial cracking and crack development of the RPC layer, shown in Tables 5 and 6 and Figs. 21 and 22, indicated that the sawtooth wet joint, rectangular wet joint, and steel plate–enhanced wet joint had a substantially better crack resistance performance than the conventional wet joint, and they had crack resistance performance as good as that of the integral casting detail in the tensile test series on panels. The reason was that the sawtooth wet joint and the rectangular wet joint prevented the direct application of the tensile load on the wet joint interfaces, whereas the specially shaped steel plate enhanced its wet joint greatly. In contrast, the conventional wet joint, inclined wet joint, and reinforcement-enhanced wet joint had small cracking stresses because of their plane interfaces. Compared with the conventional wet joint and the inclined wet joint, the crack development of the reinforcement-enhanced wet

joint was more limited because of the larger full-length reinforcements.

The theory of Mohr's circle can further explain the good crack resistance performance of the sawtooth wet joint and the rectangular wet joint. As shown in Fig. 23, the magnitude of the normal tensile stress σ_n at a plane passing through a point under a longitudinal tensile stress σ_x is given by

$$\sigma_n = \sigma_x \cos^2\theta = \frac{\sigma_x}{1+\tan^2\theta} \tag{3}$$

where θ is the rotation angle of the plane and $\tan\theta$ is the slope of the plane.

The slope of the sawtooth wet joint interface was 2:1; thus, the interface normal stress in the sawtooth wet joint was only 1/5 of the longitudinal tensile stress. Additionally, according to Eq. (3), only shear stress transferred in the vertical interfaces of the rectangular wet joint. Because the wet joint interface was more unfavorable under normal tensile stress than under shear stress, the crack resistance performance of the wet joint could be improved by using sawtooth or rectangular interfaces. Additionally, it should be noted that although the inclined wet joint also had decreased normal tensile stress on the inclined surface according to Eq. (3), its crack resistance performance was not as good as that of the sawtooth wet joint because its straight boundary line in the RPC surface facilitated the crack opening.

The crack development comparisons of the panels with the beams are shown in Fig. 24. The solid and dashed lines represent the nominal RPC tensile stress–maximum crack width curves of the panels and beams with the same wet joint detail. The figure indicates that the maximum crack width developed faster in the tensile test series on panels than in the bending test series on beams. This can be explained by the different load patterns of the two test series. In the tensile test series on panels, the RPC layer was subjected to direct tensile load, so the load pattern was similar to that in the pure tensile test of the RPC material; in the bending test series on beams, however, the tensile force was transmitted to the RPC layer by shear connectors through bending, so part of the stress in RPC was redistributed into the steel elements after initial cracking. Therefore, the RPC layer in the tensile test series on panels was subjected to more unfavorable load and developed wider cracks than that in the bending test series on beams under the same normal RPC tensile stress.

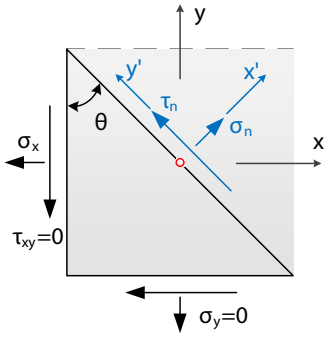

Fig. 23. Stress components at a plane passing through a point under longitudinal tensile stress

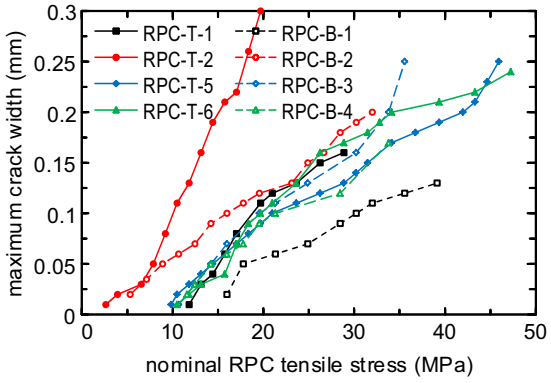

Fig. 24. Crack development comparisons of panels with beams

Durability-Based Allowable RPC Tensile Stress

According to Schmidt and Fehling (2005), the uncracked stage in the stress–strain relation of RPC is limited by the tensile strength of the cement matrix, and as a result, the cracking stress of fiber-reinforced RPC was not different from that of nonfiber-reinforced RPC. However, according to this study, the postcracking behavior was improved significantly. A typical load-deflection curve in the PRC four-point bending material test (Fig. 25) showed that the modulus of RPC did not decrease notably in the microcracking stage because the RPC layer could still bear the tensile load with the steel fibers. Additionally, the load-deformation curves of the test models (Figs. 13 and 17) suggested that their stiffness did not decrease greatly after initial cracking. Therefore, as long as the durability requirements are satisfied, the initial cracking of the RPC layer can be allowed in bridge designs.

According to Rafiee (2012), the RPC critical crack width for durability is approximately 0.05 mm. When the crack width is less than the critical width, RPC behaves as a sound material from the viewpoint of durability. Thus, this durability-based RPC critical width design criteria may be applied. Because the modulus of RPC did not decrease notably in the microcracking stage, the assumptions for calculating the nominal RPC tensile stress are still valid. Therefore, an allowable RPC tensile stress can be defined as the nominal RPC tensile stress when the maximum crack width is 0.05 mm.

Calculation results of the allowable RPC tensile stresses are shown in Table 7. The allowable RPC tensile stresses for the integral casting detail according to the tensile tests on panels and the bending tests on beams were 15.1 and 17.8 MPa, respectively, whereas the maximum allowable RPC tensile stresses for wet joints according to the two test series were 16.4 and 14.2 MPa,

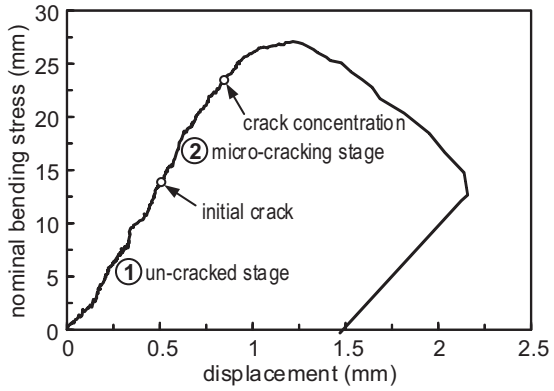

Fig. 25. A typical load-deflection curve in the PRC four-point bending material test

Table 7. Durability-Based Allowable RPC Tensile Stresses

Detail	Tensile tests on panels		Bending tests on beams	
	$\sigma_{cr,t}$ (MPa)	$\sigma_{a,t}$ (MPa)	$\sigma_{cr,b}$ (MPa)	$\sigma_{a,b}$ (MPa)
Integral casting detail	11.8	15.1	16.0	17.8
Conventional wet joint	2.6	7.9	5.3	8.9
Reinforcement-enhanced wet joint	7.9	11.8	—	—
Inclined wet joint	6.6	9.8	—	—
Sawtooth wet joint	9.8	14.4	10.7	14.2
Rectangular wet joint	10.5	16.4	11.6	14.2
Steel plate–enhanced wet joint	10.5	15.7	—	—

Note: $\sigma_{a,t}$ = the allowable RPC tensile stress according to the tensile tests on panels; $\sigma_{a,b}$ = allowable RPC tensile stress according to the bending tests on beams.

respectively, when using rectangular-shaped interfaces. The allowable RPC tensile stress results from the two test series match each other well, and thus validate each other from another perspective. Additionally, Table 7 indicates that the allowable RPC tensile stresses were considerably larger than the cracking stresses. Therefore, the RPC initial cracking-based bridge design is too conservative. For more economical bridge designs, the durability-based allowable RPC tensile stress should be applied, and use of the average of the results from the two test series is recommended.

Conclusions

In this study, seven panels and four beams were designed and tested to investigate the tensile behavior of RPC wet joints in a prefabricated composite bridge deck system. The main conclusions are summarized as follows:

1. The mechanical properties of different wet joint details were close to one another. In comparisons of the load-deformation curves of the models in each test series, no significant difference was found.
2. The crack resistance performance of different wet joint details differed considerably. Comparisons of the nominal RPC tensile stress–maximum crack width curves indicated that the sawtooth wet joint, rectangular wet joint, and steel plate–enhanced wet joint had substantially better crack resistance performance than the conventional wet joint. In contrast, the inclined wet joint and the reinforcement-enhanced wet joint had poor crack resistance performance because of their plane interfaces. Therefore, in the design of a prefabricated composite deck system, a wet joint with sawtooth- or rectangular-shaped interfaces is recommended, and the specially shaped steel plate can also be applied to further enhance the wet joint.
3. The load patterns of the tensile tests on panels and the bending tests on beams were different. The RPC layer in the tensile tests on panels was subjected to more unfavorable load, and its maximum crack width developed faster.
4. For more economical bridge designs, the durability-based allowable RPC tensile stress should be applied instead of the initial cracking stress. References can be made to Table 7 for the allowable RPC tensile stresses of different wet joint details.
5. The shear slip effect of the shear connectors may be important to the design of the RPC layer on a composite deck system. Therefore, in the bridge design, a similar partial-interaction analysis should be conducted to decide whether or not this shear slip effect should be considered.

Acknowledgments

The authors gratefully acknowledge the financial support provided by the National Science Fund of China (Nos. 51138007 and 51229801). The authors also express their sincere appreciation to the reviewers of this paper for their constructive comments and suggestions.

References

AASHTO. (2012). *AASHTO LRFD bridge design specifications*, 6th Ed., Washington, DC.

An, L., and Cederwall, K. (1996). "Push-out tests on studs in high strength and normal strength concrete." *J. Constr. Steel Res.*, 36(1), 15–29.

Bărbos, G. A., and Păstrav, M. (2014). "State-of-the-art report on ultra-high performance concrete (UHPC)." *Constructii*, 15(1), 63–69.

Buitelaar, P., Braam, R., and Kaptijn, N. (2004). "Reinforced high performance concrete overlay system for rehabilitation and strengthening of orthotropic steel bridge decks." *Proc., 1st Int. Orthotropic Bridge Conf.*, ASCE, Reston, VA, 384–401.

Connor, R., et al. (2012). "Manual for design, construction, and maintenance of orthotropic steel deck bridges." *FHWA-IF-12-027*, Federal Highway Administration, U.S. DOT, Washington, DC.

de Jong, F. B. P. (2004). "Overview fatigue phenomenon in orthotropic bridge decks in the Netherlands." *Proc., 1st Int. Orthotropic Bridge Conf.*, ASCE, Reston, VA, 489–512.

Hulsey, J., Yang, L., and Raad, L. (1999). "Wearing surfaces for orthotropic steel bridge decks." *Transportation Research Record*, 1654, 141–150.

Johnson, R. P. (2004). *Composite structures of steel and concrete: Beams, slabs, columns, and frames for buildings*, 3rd Ed., Blackwell Scientific Publications, Oxford, U.K.

Li, V. C., Stang, H., and Krenchel, H. (1993). "Micromechanics of crack bridging in fibre-reinforced concrete." *Mater. Struct.*, 26(8), 486–494.

Nie, J., Fan, J., and Cai, C. S. (2004). "Stiffness and deflection of steel-concrete composite beams under negative bending." *J. Struct. Eng.*, 10.1061/(ASCE)0733-9445(2004)130:11(1842), 1842–1851.

Rafiee, A. (2012). "Computer modeling and investigation on the steel corrosion in cracked ultra high performance concrete." Structural materials and engineering series No. 21, Kassel University Press GmbH, Kassel, Germany.

Richard, P., and Cheyrezy, M. (1995). "Composition of reactive powder concretes." *Cem. Concr. Res.*, 25(7), 1501–1511.

Schmidt, M., and Fehling, E. (2005). "Ultra-high-performance concrete: research, development and application in Europe." *ACI Special Publication*, 228, 51–78.

Shao, X., Yi, D., Huang, Z., Zhao, H., Chen, B., and Liu, M. (2013). "Basic performance of the composite deck system composed of orthotropic steel deck and ultrathin RPC layer." *J. Bridge Eng.*, 10.1061/(ASCE)BE.1943-5592.0000348, 417–428.

Walter, R., Olesen, J. F., Stang, H., and Vejrum, T. (2007). "Analysis of an orthotropic deck stiffened with a cement-based overlay." *J. Bridge Eng.*, 10.1061/(ASCE)1084-0702(2007)12:3(350), 350–363.

Wang, Y. C. (1998). "Deflection of steel-concrete composite beams with partial shear interaction." *J. Struct. Eng.*, 10.1061/(ASCE)0733-9445(1998)124:10(1159), 1159–1165.

Wolchuk, R. (1963). *Design manual for orthotropic steel plate deck bridges*, AISC, Chicago.

Wolchuk, R. (1999). "Steel orthotropic decks developments in the 1990s." *Transportation Research Record*, 1688, 30–37.

Wolchuk, R. (2002). "Structural behaviour of surfacings on steel orthotropic decks and considerations for practical design." *Struct. Eng. Int.*, 12(2), 124–129.